

PRACTICAL SUPERCONDUCTOR DEVELOPMENT
FOR ELECTRICAL POWER APPLICATIONS
ARGONNE NATIONAL LABORATORY

QUARTERLY REPORT FOR THE PERIOD ENDING SEPTEMBER 30, 2001

This is a multiyear experimental research program that focuses on improving relevant material properties of high- T_c superconductors (HTSs) and developing fabrication methods that can be transferred to industry for production of commercial conductors. A key element of this Argonne National Laboratory (ANL) program is the development of teaming relationships with industrial partners in the areas of conductor development and prototype electric power system product demonstration.

Technical Highlights

Recent results are presented on the fabrication and characterization of $\text{YBa}_2\text{Cu}_3\text{O}_x$ (YBCO)-coated conductors that are made by two approaches. In one approach, YBCO is deposited by pulsed laser deposition (PLD) on a biaxially textured MgO substrate prepared by inclined substrate deposition (ISD); in the other approach, YBCO is deposited directly onto silver substrates by ISD. We also present results on an analysis of residual stresses in coated conductors, and describe the use of Raman microscopy to analyze the c-axis alignment and residual strains in coated conductor films.

Fabrication of Coated Conductors

YBCO on ISD MgO

Biaxially textured MgO thin films were deposited on mechanically polished Hastelloy C276 (HC) substrates by the ISD method. This deposition was accomplished by e-beam evaporation in an experimental setup described elsewhere [1]. The inclination α (see Fig. 1) is defined as the angle between the substrate normal and the evaporation direction. In these depositions, α was varied between 10 and 70°. Oxygen flow was introduced into the system to maintain an operating pressure of 2×10^{-5} torr during film deposition. A quartz crystal monitor was mounted beside the sample stage to monitor the deposition rate. High deposition rates of 20-100 Å/s were used, and the substrate temperature was maintained between room temperature and 50°C during deposition.

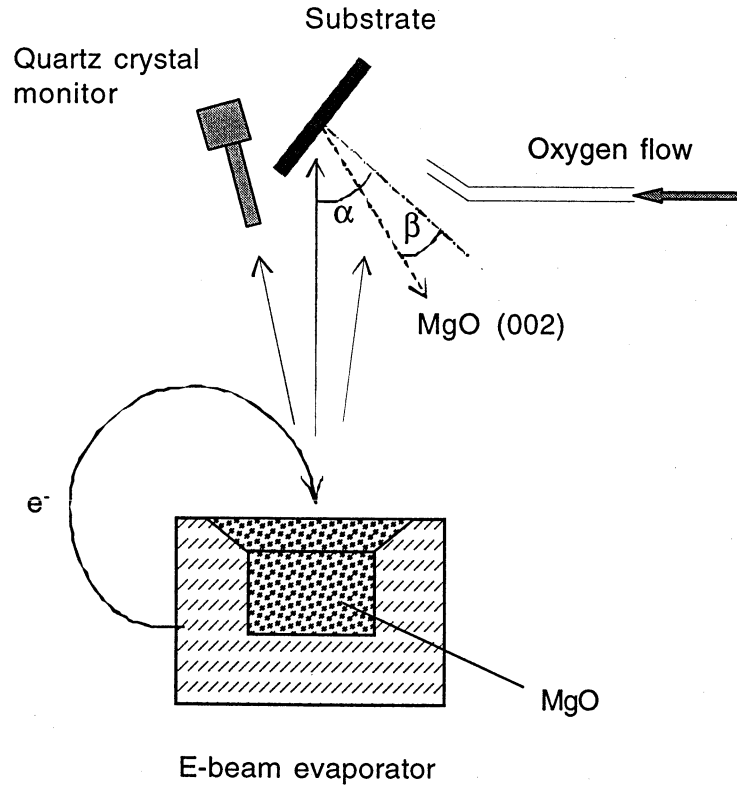


Fig. 1. Experimental arrangement for inclined substrate deposition (ISD) of MgO on HC substrate.

To decrease the surface roughness of the as-deposited ISD MgO films, an additional thin (0.2-0.5 μm) layer of MgO was deposited at an elevated temperature (700-800 $^{\circ}\text{C}$) and an inclination of $\alpha = 0^{\circ}$. To improve the lattice match with YBCO, thin layers of yttria-stabilized zirconia (YSZ) and ceria were deposited on top of the MgO. Subsequently, YBCO films were deposited by PLD on these ISD-MgO-buffered substrates using an excimer laser system (Lambda Physik COMPex 201). Substrates were attached to the sample stage with silver paste, and the substrate temperature was controlled at 700-800 $^{\circ}\text{C}$ during the deposition of YBCO.

Surface morphology and crystalline orientation of the films were investigated by scanning electron microscopy (SEM) and transmission electron microscopy (TEM). Surfaces were examined by atomic force microscopy (AFM) using a Digital Instrument NanoScope. The texture of the films was characterized by X-ray pole figures, ϕ -scans and ω -scans. To make transport measurements, samples were first coated with 2- μm -thick silver by e-beam evaporation and then annealed in flowing high-purity oxygen at 400 $^{\circ}\text{C}$ for 2 h.

Plan-view SEM revealed (Fig. 2a) a "roof-tile" structure for an ISD MgO film that was deposited at room temperature with $\alpha = 55^\circ$. A cross-sectional fracture surface showed columnar grains that were nearly perpendicular to the substrate surface (Fig. 2b). The MgO grain size increased with film thickness for thicknesses $<0.25 \mu\text{m}$, but stabilized at $\approx 0.1 \mu\text{m}$ for thicknesses $>0.25 \mu\text{m}$.

Figure 3 shows the MgO (002) and (220) X-ray pole figures for an ISD MgO film (thickness $\approx 1.5 \mu\text{m}$) that was deposited at room temperature with $\alpha = 55^\circ$. The sharp, well-defined poles (Fig. 3a) for the [001] axis as well as the [010] and [100] axes indicate that the film exhibits good biaxial texture. The asymmetric distribution of the pole peaks reveals that the MgO (00 l) planes are tilted with respect to the substrate normal. The tilt angle, β , is determined from the χ -angle value of the [001] reflection in the MgO (002) pole figure; $\beta = 32^\circ$ for the ISD MgO film deposited at room temperature with an inclination of 55° .

The in-plane and out-of-plane textures of the ISD MgO films were characterized with the MgO (002) ϕ - and ω -scans taken at the [001] pole. The full width at half-maximums (FWHMs) for the ϕ - and ω -scans of this MgO film were 12.2° and 6.3° , respectively. After depositing a homoepitaxial layer of MgO ($0.5\text{-}\mu\text{m}$ thick) on the ISD MgO film, these FWHMs improved to 9.2° and 5.4° for the (002) ϕ - and ω -scans, respectively, as seen in Fig. 4. The AFM analysis showed that the homoepitaxial MgO layer also decreased the RMS surface roughness from $\approx 28 \text{ nm}$ to $\approx 10 \text{ nm}$.

Figure 5 shows a TEM image and selected area diffraction (SAD) pattern of MgO columnar grains in a film that was deposited with $\alpha = 55^\circ$. The top facet of MgO grains is a (002) plane. Film morphology and texture evolution in the ISD MgO films can be understood from the self-shadowing effect. It has been demonstrated [2] that in-plane texture develops during the growth of polycrystalline films through a combination of

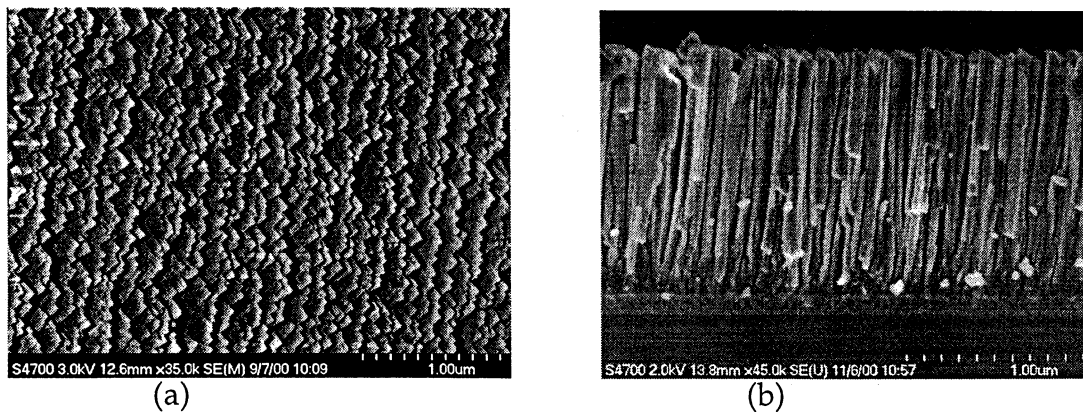


Fig. 2. (a) Plan view and (b) cross-sectional view from secondary electron images of ISD MgO film deposited with $\alpha = 55^\circ$.

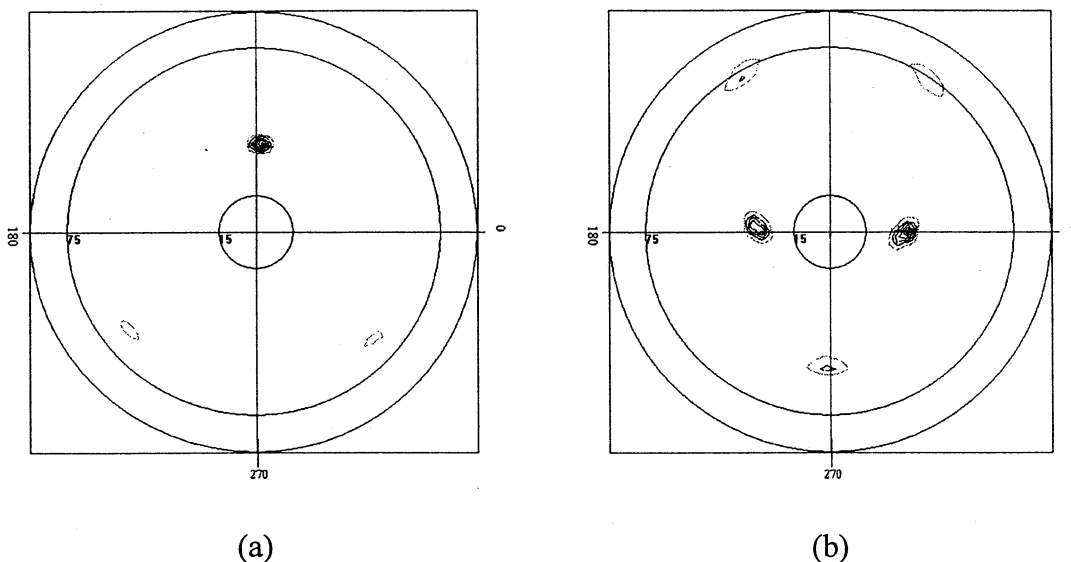


Fig. 3. (a) MgO (002) and (b) MgO (220) pole figures.

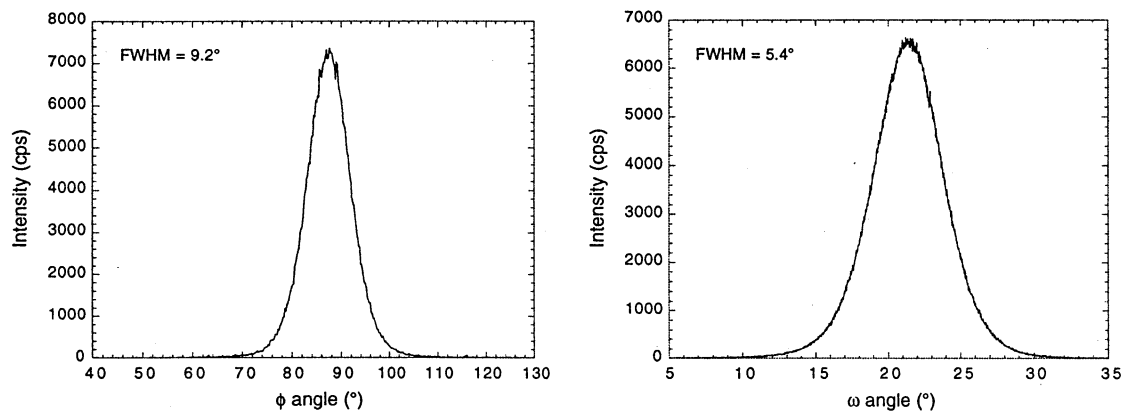


Fig. 4. (a) MgO (002) ϕ -scan and (b) MgO (002) ω -scan patterns after deposition of homoepitaxial MgO layer.

fast growth along a certain crystallographic direction and self-shadowing that results from deposition at an inclined angle. In the case of MgO, the fast growth plane is {200} [3]. Because maximizing the (002) faces can decrease the surface free energy, the {200} plane is also the equilibrium crystal habit, as confirmed by the cubic morphology exhibited in the MgO film [4]. With deposition at an inclined angle, the {200} plane rotates toward the vapor source, so that the (002) surface grows faster than other crystalline faces. Figure 6 presents a schematic representation of this grain growth mechanism.

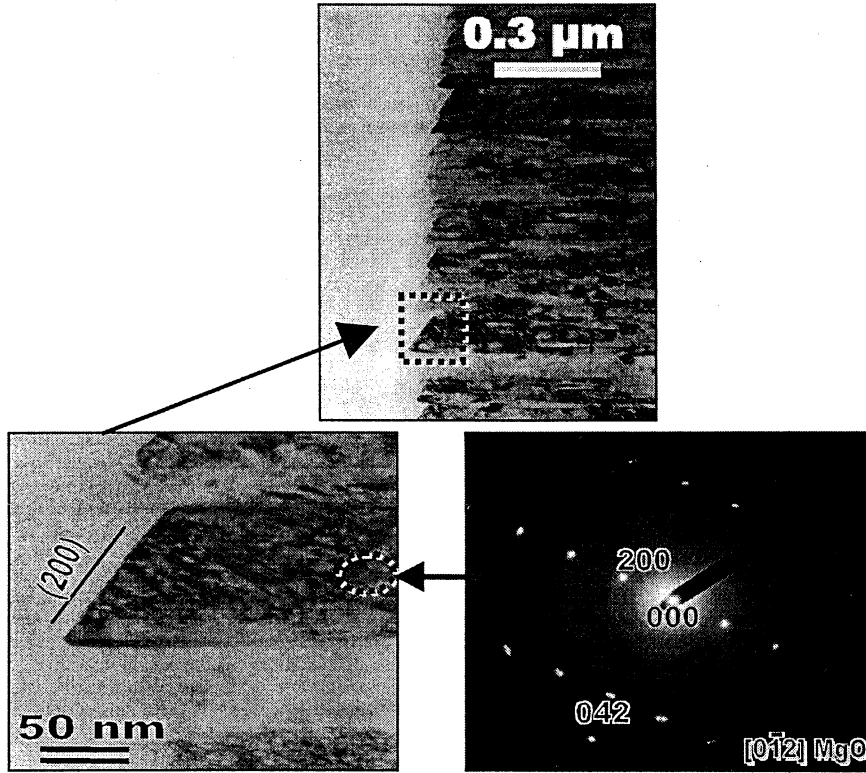


Fig. 5. Facet of (200) plane on top of MgO columnar grain and corresponding SAD pattern.

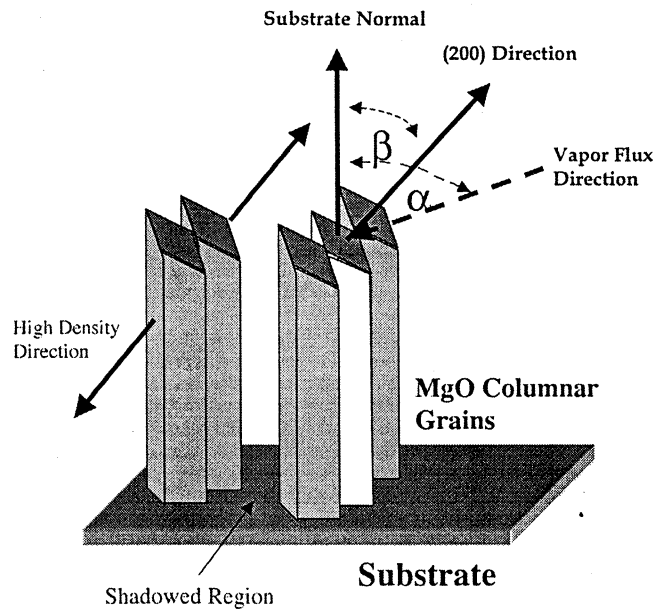


Fig. 6. Illustration of ISD MgO growth mechanism due to shadowing effect.

Biaxially aligned YBCO films were successfully deposited by PLD on ISD-MgO-buffered HC substrates. Figure 7 shows ϕ -scans for the MgO (220) and YBCO (103) grown on the MgO-buffered HC substrate; it reveals epitaxial growth, with the usual cube-to-cube biaxial alignment: YBCO [001] // MgO [001] and YBCO [100] // MgO [100] (or MgO [010]). To decrease the lattice mismatch and thereby enhance the superconducting properties of YBCO films, various buffer layers were tested. These buffer layers were deposited between the MgO and YBCO layers by either e-beam evaporation or PLD. Inductive measurements for 0.5- μm -thick YBCO on MgO-buffered HC (Fig. 8) show that $T_c = 90$ K, and the superconducting transition is complete at 88 K. The inductive measurements also showed a critical current density of $\approx 2 \times 10^5$ A/cm² at 77 K in the self-field on a sample that is 0.5- μm thick, 0.5-cm wide, and 1-cm long.

YBCO on Silver

Direct deposition of YBCO on silver (Ag) substrates has the potential to simplify the fabrication of coated conductors by eliminating the need for buffer layers. Other fabrication methods using nickel or nickel alloy substrates require multiple buffer layers to prevent cation diffusion that degrades the YBCO properties. Direct deposition of YBCO on Ag removes the need for buffer layers, because Ag is chemically inert toward YBCO under fabrication conditions.

Mechanically polished Ag pieces (1 μm finish) measuring ≈ 0.2 -mm thick, ≈ 5 -mm wide, and 10-mm long were used as substrates for ISD of YBCO films. The experimental arrangement for ISD is shown in Fig. 9, where α is the inclination

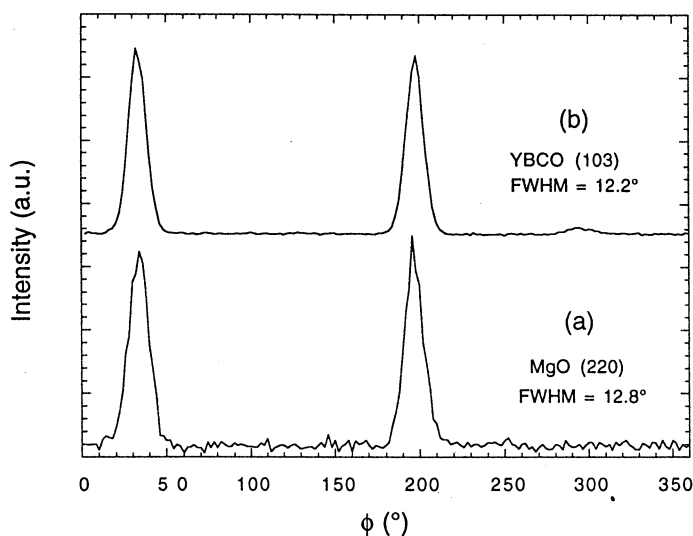


Fig. 7. ϕ -scan patterns of MgO (220) and YBCO (103) indicating epitaxial growth.

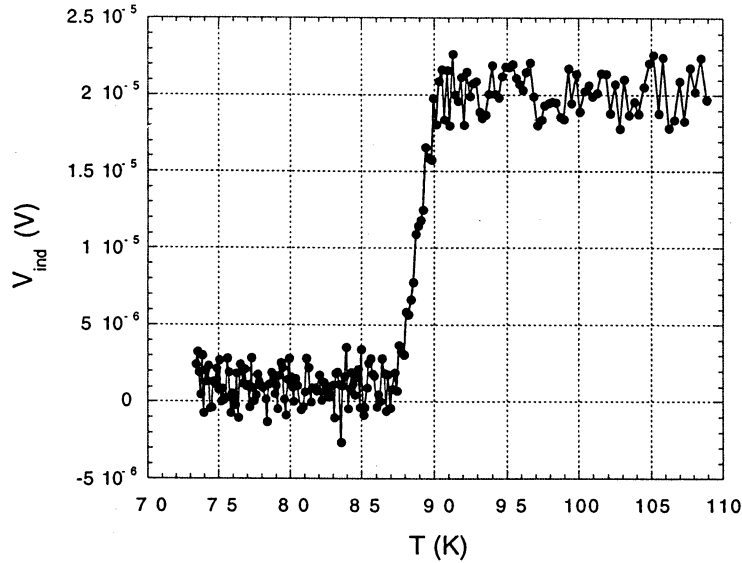


Fig. 8. Critical-temperature transition curve for YBCO film deposited on ISD-MgO-buffered HC substrate. V_{ind} is the inductive voltage.

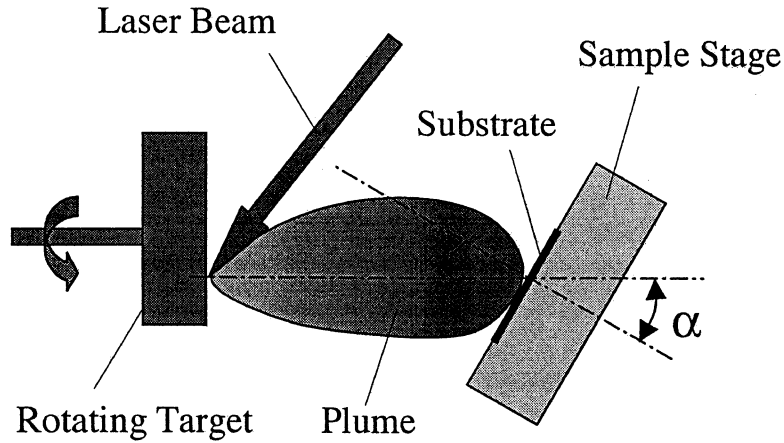


Fig. 9. Experimental setup for the inclined substrate deposition (ISD) of YBCO films directly on Ag substrates.

between the substrate normal and the axial direction of the plume. YBCO films were deposited at various inclinations using commercial YBCO targets (2.5-cm dia. x 0.6-cm thick) and a Lambda Physik LPX 200 series excimer laser with KrF as the lasing medium. The Ag substrate was attached to a temperature-controlled stage using silver paste and was kept at 700-800°C during deposition. The laser spot size on the rotating target was 3 mm², giving an energy density of 2.5-3 J/cm². The distance between the

target and the substrate was ≈ 5.5 cm. The base pressure of the chamber was 2×10^{-6} torr. High-purity oxygen flowed (≈ 10 sccm) during deposition to maintain an operating pressure of 0.1 to 0.3 torr.

X-ray diffraction pole figures were collected with a Scintag XRD 2000 diffractometer using $\text{Cu K}\alpha$ radiation. TEM was performed in a Philips CM30 microscope. Surfaces of the films were analyzed by AFM using a Digital Instrument NanoScope. The superconducting transition temperature (T_c) was measured inductively, and the transport critical current density (J_c) was measured by the four-probe method.

The surface morphology of YBCO films deposited on polished Ag substrates was examined by AFM. Unlike YBCO on single-crystal substrates, grain boundaries are clearly evident in the plan view of YBCO on Ag (Fig. 10). The film contains c-axis oriented grains with an average size of $\approx 0.5 \mu\text{m}$, as well as a few uniformly dispersed a-axis oriented grains (Fig. 10). The a-axis oriented grains were also seen by SEM (Fig. 11); however, only $(00l)$ peaks were observed in the 2-theta X-ray diffraction pattern (Fig. 12), indicating that the YBCO film had strong c-axis orientation. The strong c-axis alignment was confirmed by an intense peak at 340 cm^{-1} in the Raman

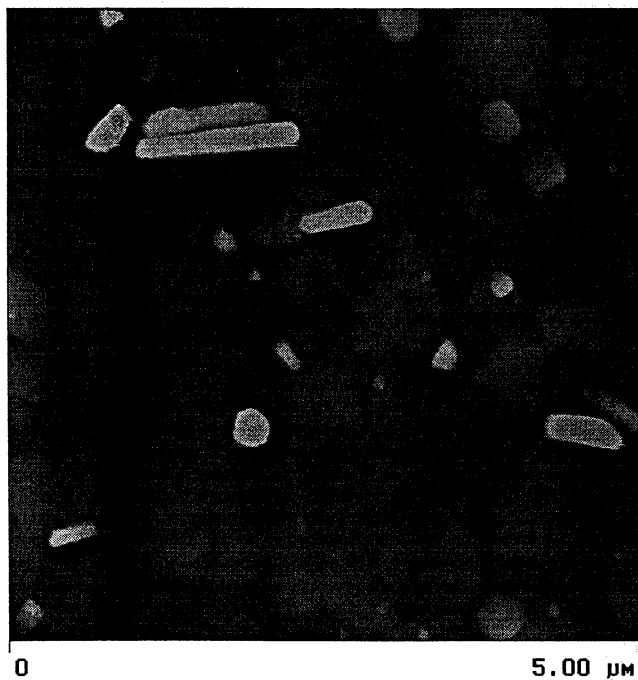


Fig. 10. Plan view by atomic force microscopy (AFM) of a YBCO film deposited directly on Ag substrate at 755°C with inclination of 55° .

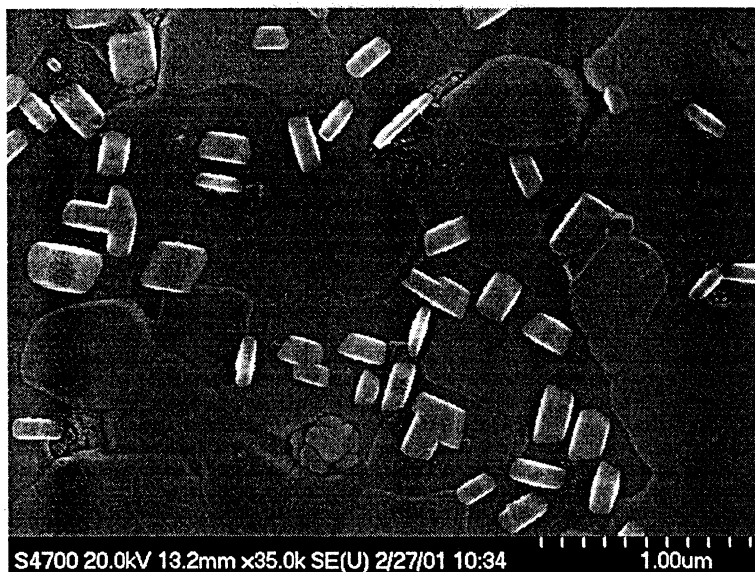


Fig. 11. Secondary electron image (plan view) of a YBCO film deposited directly on Ag substrate at 755°C with inclination of 55°.

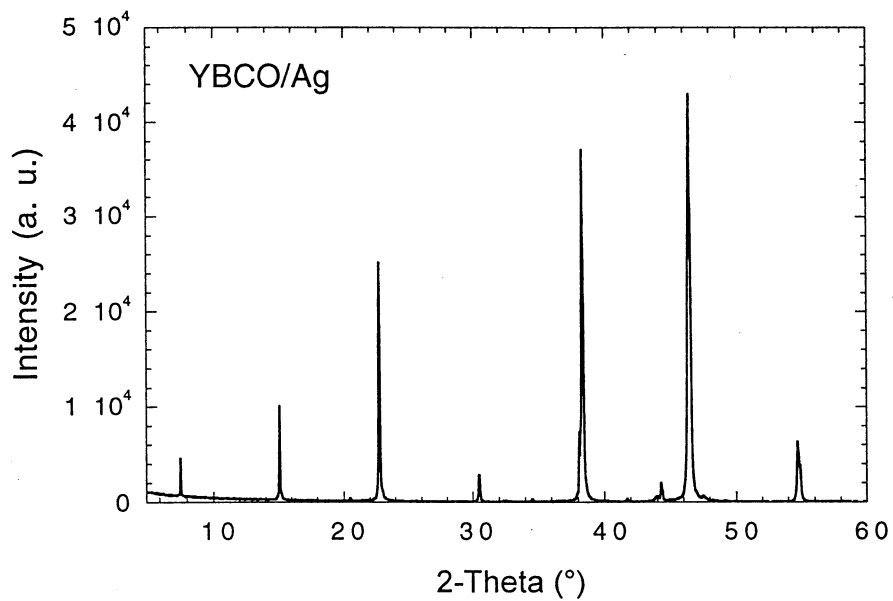


Fig. 12. A 2-theta X-ray diffraction pattern for the YBCO film deposited directly on polished Ag substrate.

spectrum (Fig. 13). The YBCO (103) pole figure (Fig. 14) revealed, however, that the YBCO on Ag had only fiber texture with its *c*-axes aligned parallel to the substrate normal. The film showed no biaxial alignment, i.e., its *a*- and *b*-axes were not preferentially aligned in the YBCO films.

Cross-sectional TEM (Fig. 15) revealed an amorphous layer at the interface between YBCO and the Ag substrate. The origin of this layer and its role in the growth of YBCO are not fully understood and are being studied further. For the sample deposited at 755°C with an inclination of 55°, the thickness of the amorphous layer was ≈70 nm. Figure 16 shows the EDS spectra of the YBCO film and the amorphous layer. The YBCO layer contained minimal Ag, while the amorphous layer contained significant concentrations of Ag, Y, Ba, and Cu. The relative concentrations varied through the thickness of the amorphous layer, with the Ag concentration decreasing and the Y, Ba, and Cu concentrations increasing closer to the YBCO film. In addition, TEM EDS indicated that the YBCO was slightly Cu-deficient, suggesting that Cu diffused into the amorphous layer or the Ag substrate. To reduce the driving force for Cu diffusion, several Ag substrates were prepared with 0.5 mol.% Cu. In future work, YBCO will be deposited on these substrates by PLD, and the effect of Cu on YBCO growth and properties will be studied.

Figure 17 shows the superconducting transition that was measured inductively for a YBCO film deposited on Ag at 755°C with an inclination of 55°. The transition was sharp with $T_c(\text{onset}) \approx 90$ K and was complete at ≈88 K. To measure the transport J_c by

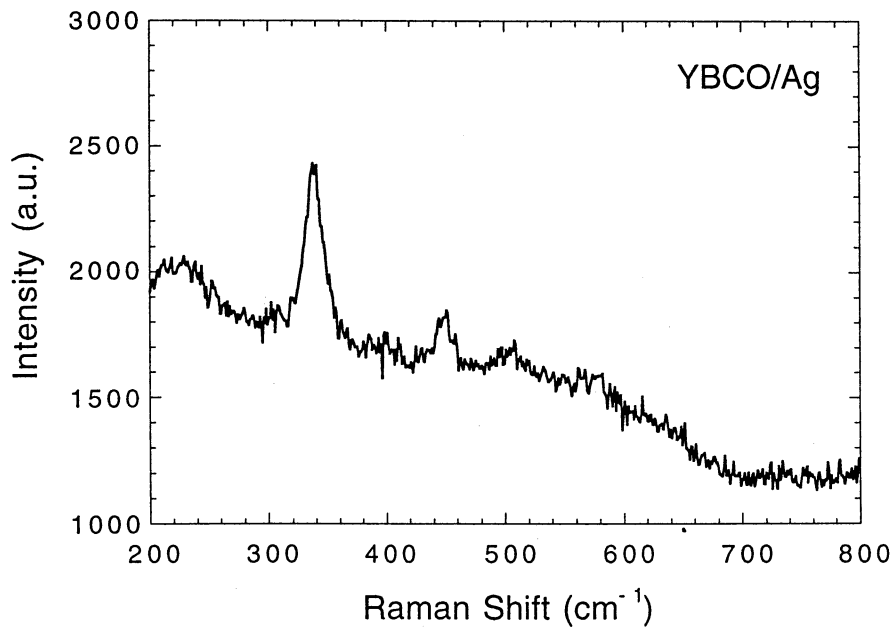


Fig. 13. Raman spectrum of a YBCO thin film deposited directly on Ag substrate.

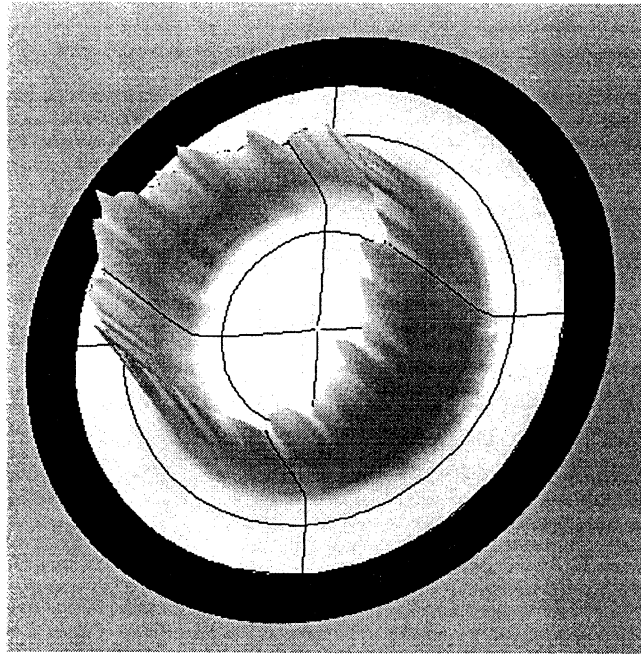


Fig. 14. (103) pole figure of a YBCO thin film deposited directly on Ag substrate.

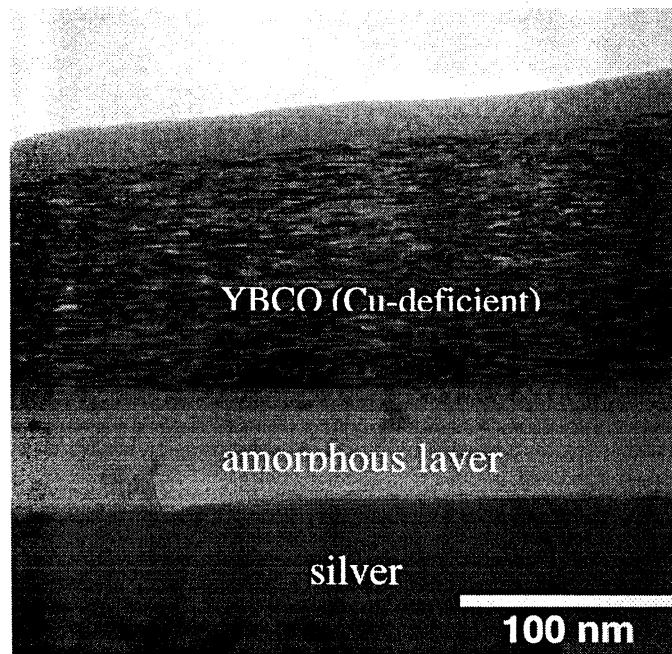


Fig. 15. Cross-sectional view (by TEM) of YBCO deposited directly on Ag substrate at 755°C with an inclination of 55°.

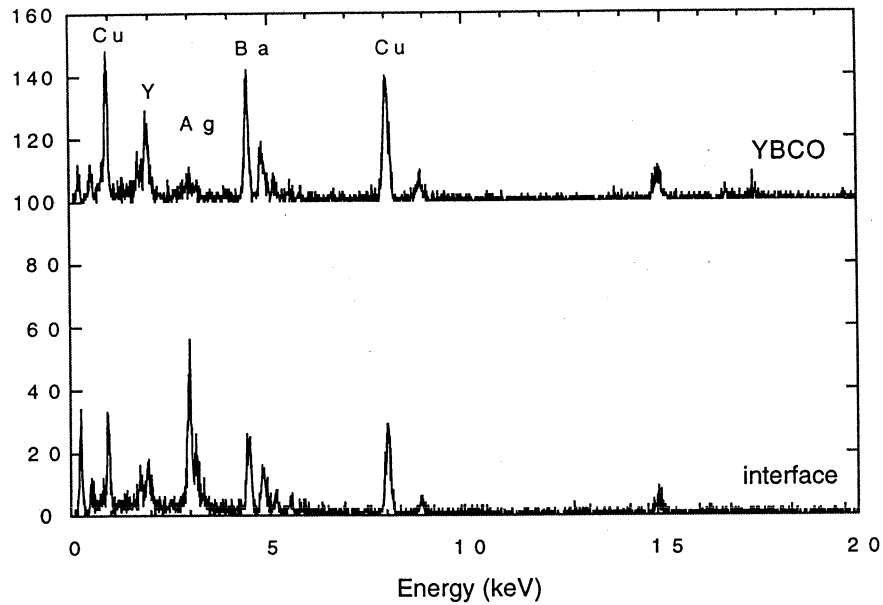


Fig. 16. TEM EDS spectra of the YBCO film deposited directly on Ag and the amorphous layer at the interface between Ag and YBCO.

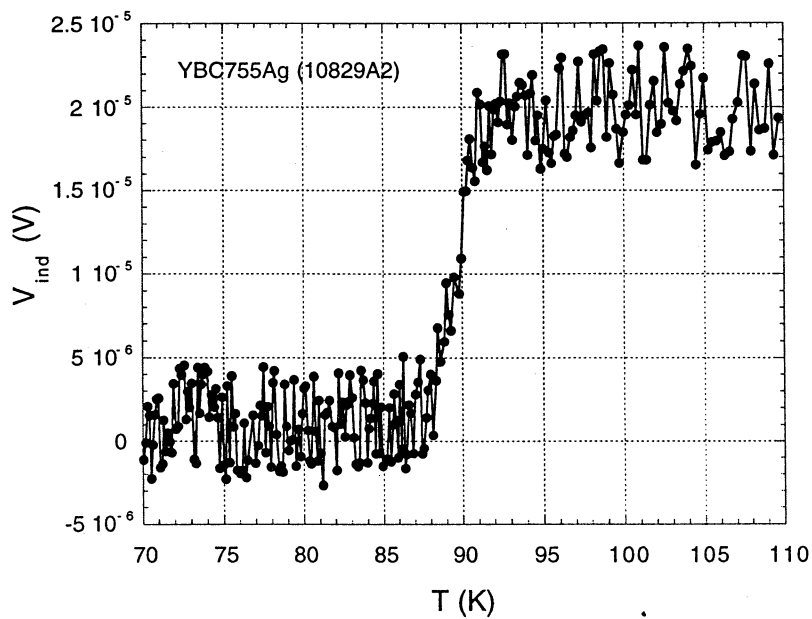


Fig. 17. Superconducting transition curve of YBCO film deposited directly on Ag at 755°C, as determined by inductive method.

the four-probe method, the YBCO/Ag samples were coated with Ag ($\approx 2\text{-}\mu\text{m}$ thick) by e-beam evaporation, then were annealed in flowing high-purity oxygen at 400°C for 2 h. For YBCO deposited at 755°C with an inclination of 55° , the data in Fig. 18 indicate that $J_c(\text{transport}) = 275,000 \text{ A/cm}^2$ at 77 K in the self-field using the $1 \mu\text{V/cm}$ criterion. Figure 19 shows $T_c(\text{onset})$ for multiple samples deposited at inclinations of 35 , 55 , and 72° . The data are quite scattered, but the highest T_c was obtained on a sample deposited with an inclination of 55° .

Analysis of Residual Stresses

The residual stresses in ZrO_2 and YBCO films on HC and LaAlO_3 (LAO) substrates were previously estimated with an X-ray diffraction technique [5]. The stresses were calculated from residual strains that were obtained by measuring the lattice parameters of stressed and stress-free films. To confirm the validity of this technique and the resulting stress evaluation, the stresses in these films were measured by an independent technique based on curvature measurements using 3-D optical interferometry. In this report, we use these curvature measurements to estimate the residual stress in a YBCO film on an LAO substrate.

To make the curvature measurement, flat LAO substrates ($150\text{-}\mu\text{m}$ thick) were prepared by polishing them on both sides. The initial curvature of the polished substrates was measured by optical interferometry. Several measurements were made to improve the statistical reliability. The polished substrates were then coated with YBCO ($0.3\text{-}\mu\text{m}$ thick) by PLD, and the curvature of the coated surfaces was measured by optical interferometry. The difference in curvature before and after coating with YBCO gives the coating curvature due to residual stress. This curvature was used to calculate the residual stress (σ) by modification of Stoney's equation [6].

The average residual stress measured on five specimens was $210 \pm 72 \text{ MPa}$. This compares very well with the value of $178 \pm 53 \text{ MPa}$ that was measured by X-ray diffraction and reported previously [5]. The good agreement between the results confirms the validity of the measurement technique. Further studies using optical interferometry are in progress to evaluate the residual stresses in different coated-conductor architectures.

Analysis of c-Axis Alignment and Stress using Raman Microscopy

Work is in progress to develop rapid, accurate, and (where possible) in situ methods for characterizing the phase chemistry and microstructure of coated conductor embodiments. As discussed in previous progress reports, Raman microscopy is proving to be a very useful tool for measuring a variety of coated conductor characteristics, including oxygen stoichiometry, cation disorder, the presence and spatial distribution of second phases, c-axis verticality, and relative strain levels. During the past reporting

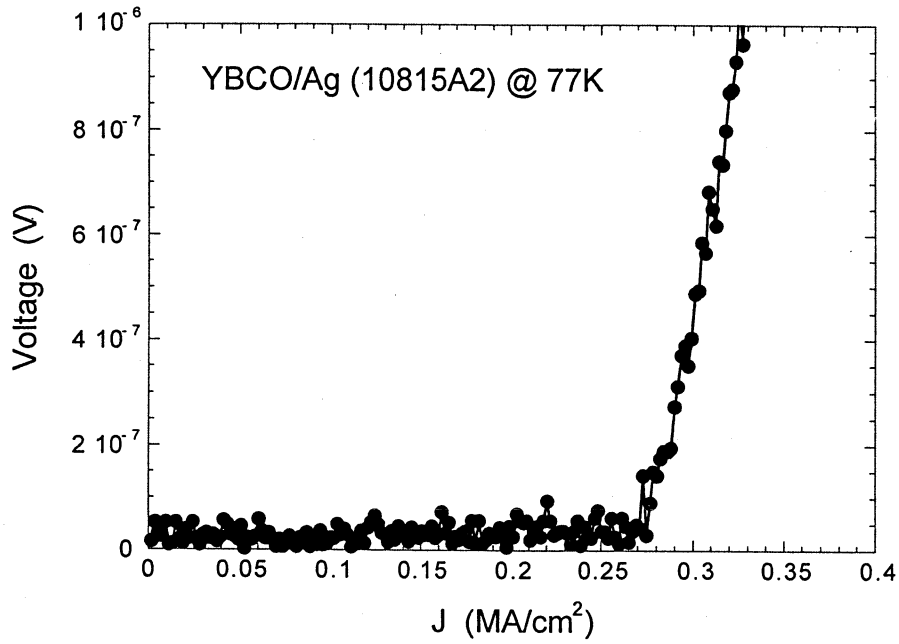


Fig. 18. J_c transition curve in self-field for a YBCO film deposited directly on Ag at 755°C.

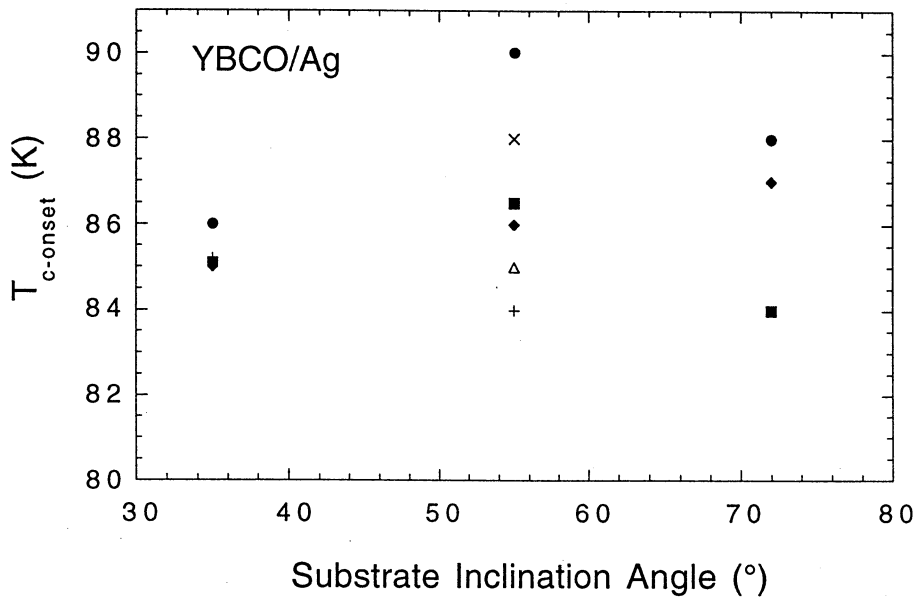


Fig. 19. Critical transition temperature, T_c , of YBCO films on silver as a function of substrate inclination.

period, we have used Raman microscopy to develop spatial maps that gauge the c-axis alignment of the grains in YBCO films grown on textured substrates. As a result of inherent differences in the polarization tensors for the Raman active phonons of YBCO, the out-of-phase O2/O3 mode of YBCO at ca. 340 cm^{-1} reaches maximum intensity, while the O4 mode at ca. 500 cm^{-1} reaches minimum intensity when the excitation laser is brought to the sample surface in a direction perpendicular to the YBCO c-axis. As the c-axis tips with respect to the incident laser line, the $I(500)/I(340)$ intensity ratio rapidly increases, thus providing a measure of the degree of YBCO c-axis tilt with respect to the incident laser. As long as the direction of propagation of the laser remains perpendicular to the substrate surface, the $I(500)/I(340)$ intensity ratio can, in principle, be used to measure the extent of c-axis tilt relative to the substrate surface.

An example of two common conditions that illustrate this effect is given in Fig. 20. The top spectrum was obtained from a YBCO film deposited by PLD onto an MgO template layer that was applied to an HC substrate by ISD. The bottom spectrum is for the same embodiment except that the MgO template layer was applied by ion beam assisted deposition (IBAD). Both spectra were recorded with the propagation direction of the excitation laser perpendicular to the surface of the HC substrate. The significantly enhanced intensity of the 500 cm^{-1} mode relative to the 340 cm^{-1} mode in the top spectrum evidences the tilt of the YBCO grains caused by the inclination pitch of the ISD template. In the IBAD sample, the YBCO grains lie flat on the substrate surface (c-axis vertical); hence, the intensity of the 500 cm^{-1} mode is near its minimum, as expected. Efforts are underway to correlate the $I(500)/I(340)$ intensity ratio with the measured values of the ISD inclination angle and transport J_c .

The utility of the Raman microprobe technique for probing the spatial variation of the c-axis alignment is illustrated in Fig. 21, which maps the $I(500)/I(340)$ intensity ratio for an ISD-templated YBCO (PLD) film. The surface of evolution seen in Fig. 21 was determined by creating a contour map of 11 systematically spaced measurements on a 3 mm by 10 mm specimen. For a perfectly textured ISD sample, we would expect this surface to be flat, parallel to the (x,y) plane, and finite in value, depending on the ISD tilt angle. The particular sample represented in Fig. 21 shows evidence of a finite tilt angle in all locations, but the tilt angle is not uniform. We are in the process of recording these c-axis verticality contours for a series of ISD-templated YBCO specimens in order to investigate their connection with specimen preparation and performance.

Provoost et al. [7] have reported on the utility of Raman microspectroscopy for measuring relative strain in textured YBCO specimens. Following up on the implications of their work concerning strain fields in YBCO grains adjacent to nonsuperconducting second phase (NSP) crystallites, we have investigated the spatial dependence of the frequency of the YBCO O4 phonon in a melt-textured orthorhombic

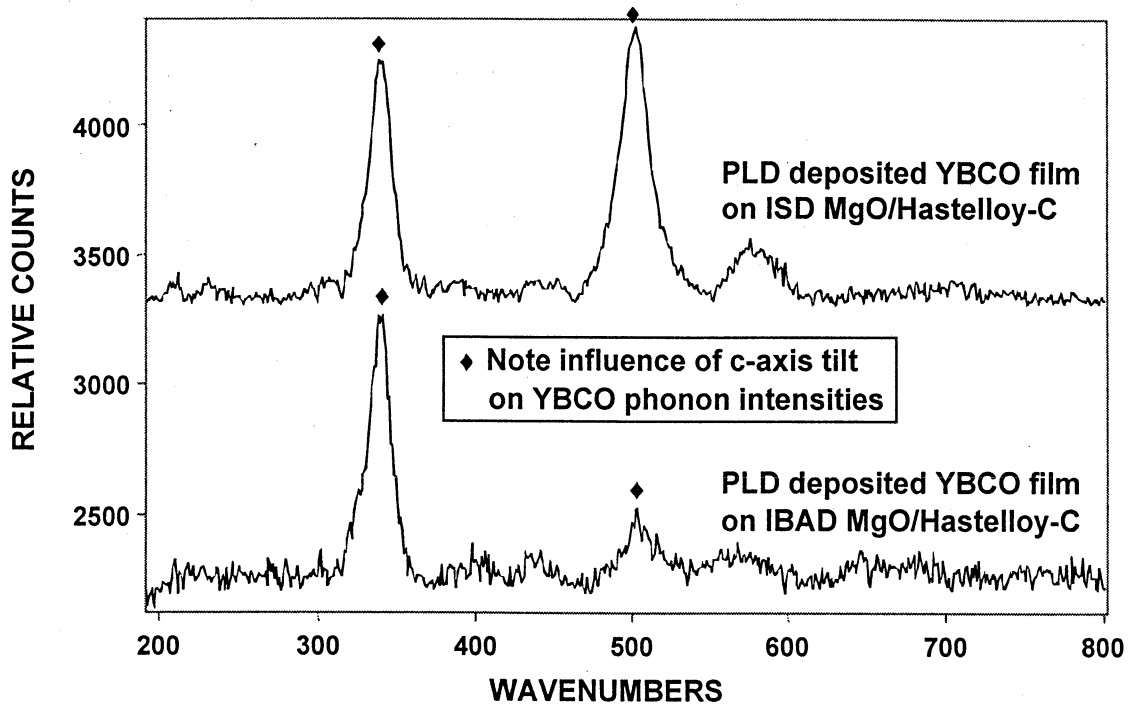


Fig. 20. Raman microprobe spectra of YBCO films on templates prepared by inclined substrate deposition (top spectrum) and ion beam assisted deposition (bottom spectrum). The direction of propagation of the excitation laser is perpendicular to the substrate in both cases.

YBCO boule containing Y_2BaCuO_5 (211) precipitates of various sizes and shapes. As the results in Fig. 22 show, the O4 phonon softens in the vicinity of NSPs, and furthermore, the extent of softening appears to depend on the shape and orientation of the NSP. Since the O4 phonon is purely a c-axis mode, its softening implies that the c-axis of YBCO grains is in greater tension near NSPs than in domains of pure YBCO. The implication is that the a-b planes of YBCO are experiencing greater compression near NSPs than in the pure YBCO domains. The determination of absolute strain levels by this method is complicated by the fact that the frequencies of the YBCO phonons (particularly the O4 phonon) are also sensitive to the oxygen stoichiometry of YBCO. Even if one accepts the assumption that all of the YBCO present in a particular sample is at the same oxygen stoichiometry value, the results in Fig. 22 only allow one to make conclusions about relative strain. We are attempting to resolve this complication by using a combination of X-ray diffraction and Raman microspectroscopy, wherein an oxygen stoichiometry calibration is made that employs data from well-characterized, annealed single crystals of YBCO. Our intention is to adapt this calibrated approach for the measurement of strain in YBCO-coated conductor embodiments.

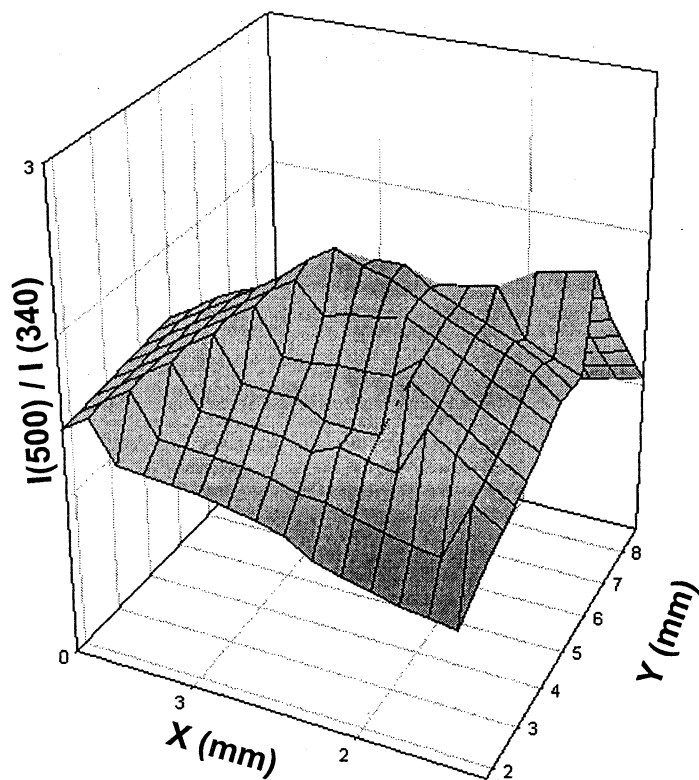


Fig. 21. Contour plot of the $I(500)/I(340)$ intensity ratio for an ISD-templated YBCO (PLD) specimen determined from 11 equi-spaced Raman microprobe measurements within the borders of the YBCO-coated region (3 mm x 10 mm).

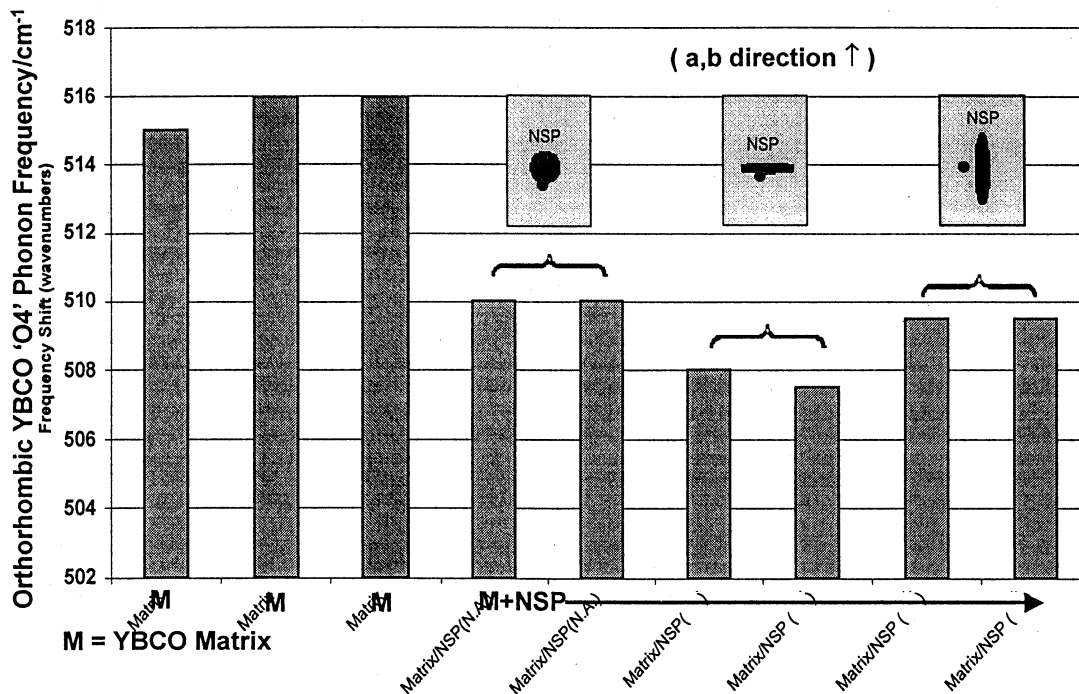


Fig. 22. Frequency histogram for the O4 phonon of YBCO domains in a melt processed sample. Locations indicated by "M" are in domains that are relatively distant from any nonsuperconducting second phase (NSP) crystallites; those indicated by "M+NSP" are near NSPs of varying shape and orientation. For non-aspected NSPs, comparable YBCO O4 phonon frequencies are observed in all adjacent regions. For aspected NSPs, the measurements were made at locations adjacent to the long surface of the crystallite.

References

1. B. Ma, M. Li, Y. A. Jee, R. E. Koritala, B. L. Fisher, and U. Balachandran, in press, *Physica C* (2001).
2. O. P. Karpenko, J. C. Bilello, and S. M. Yalisove, *J. Appl. Phys.*, 82, 1397-1403 (1997).
3. A. F. Moodie and C. E. Warble, *J. Crystal Growth*, 10, 26-38 (1971).
4. R. E. Koritala, M. P. Chudzik, Z. Luo, D. J. Miller, C. R. Kannewurf, and U. Balachandran, *IEEE Trans. on Appl. Supercond.*, 11, 3473-3476 (2001).
5. Quarterly Report for the Period Ending June 30, 2001, Practical Superconductor Development for Electrical Power Applications.

6. G. Stoney, *Proc. R. Soc. London, Ser. A*, 82, 172 (1909).
7. R. Provoost et al., *Appl. Supercond.*, 6, 185-192 (1998).

Interactions

John Hull attended the 3rd International Workshop on Processing and Applications of Superconducting (RE)BCO Large Grain Materials, July 11-13, 2001, Seattle, WA.

Beihai Ma, Meiya Li, Rachel Koritala, John Hull, Y.S. Cha, and U. Balachandran attended the ICMC/CEC conference in Madison, WI, July 16-20, 2001.

Vic Maroni, Ken Gray, John Hull, Steve Dorris, and Balu Balachandran attended the HTSC Annual Peer Review in Washington DC, Aug. 1-3, 2001.

V. Selvamanickam (IGC-SuperPower) and Brian Newnam (LANL) visited Argonne on Aug. 22, 2001 to review the IGC-SuperPower CRADA program.

U. Balachandran attended the European Conference on Applied Superconductivity (EUCAS), Copenhagen, Denmark, Aug. 26-30, 2001. He also visited the 30-m long Danish HTSC cable site at a substation in Copenhagen.

Jodi Reeves, IGC-SuperPower, visited Argonne during Aug. 29-30, 2001 and held discussions with Argonne scientists in the area of fabrication and characterization of coated conductors.

List of Publications and Presentations

Published or presented:

Y. A. Jee, M. Li, B. Ma, V. A. Maroni, B. L. Fisher, and U. Balachandran, Comparison of Texture Development and Superconducting Properties of $\text{YBa}_2\text{Cu}_3\text{O}_x$ Thin Films Prepared by TFA and PLD Processes, *Physica C*, Vol. 354/4, pp. 297-303 (2001).

K. Salama (Texas Center for Superconductivity); S. P. Athur and U. Balachandran, Texturing of REBCO Using Temperature Gradient, *Physica C* 357-360 (2001) 11-19.

J. R. Hull, Energy Storage Systems, Chapter 9.5 in "Properties, Processing, and Applications of YBCO and Related Materials," eds. W. Lo and A. M. Campbell, IEE Books, Stevenage, UK (2001).

J. R. Hull, Superconducting Bearings, Chapter 9.4 in "Properties, Processing, and Applications of YBCO and Related Materials," eds. W. Lo and A. M. Campbell, IEE Books, Stevenage, UK (2001).

R. E. Koritala, B. C. Prorok, K. C. Goretta, J.-H. Park, U. Balachandran; and M. J. McNallan (U. of Illinois at Chicago), Microstructure and Mechanical Properties of Internally Oxidized Ag/1.12 at.% Mg, Abstract presented at the 2001 Intl. Cryogenic Matls. Conf., Madison, WI, July 16-20, 2001.

J.-H. Park, K. C. Goretta and U. Balachandran, Oxidation of Hastelloy C, Abstract presented at the 2001 Intl. Cryogenic Matls. Conf., Madison, WI, July 16-20, 2001.

B. Ma, Y. A. Jee, M. Li, B. L. Fisher, and U. Balachandran, Epitaxial Growth of YBCO Films on Yttria-Stabilized-Zirconia Substrates, Abstract presented at the Cryogenic Engineering Conf. and Intl. Cryogenic Matls. Conf. (CEC/ICMC), Madison, WI, July 16-20, 2001.

B. Ma, M. Li, B. L. Fisher, R. E. Koritala, and U. Balachandran, Inclined-Substrate Deposition of Biaxially Aligned Template Films for YBCO-Coated Conductors, Abstract to be presented at 10th US-Japan Workshop on High-T_c Superconductors, Santa Fe, NM, Dec. 2-5, 2001.

M. Li, B. Ma, Y. A. Jee, B. L. Fisher, and U. Balachandran, Structural Characterization of YBCO Films Fabricated on ISD MgO by Pulsed Laser Deposition, Abstract presented at the 2001 Intl. Cryogenic Matls. Conf., Madison, WI, July 16-20, 2001.

U. Balachandran, Development of YBCO-Coated Conductors for Electric Power Applications, Invited abstract presented at 5th European Conference of Applied Superconductivity, Copenhagen, Denmark, Aug. 26-30, 2001.

U. Balachandran, Development of High-T_c Superconductors for Electric Power Applications, Abstract Book for Third Intl. Workshop on Processing and Applications of Superconducting (RE)BCO Large Grain Materials, Seattle, July 11-13, 2001.

M. Li, B. Ma, Y. A. Jee, B. L. Fisher, and U. Balachandran, Structural and Electrical Properties of Biaxially Textured YBa₂Cu₃O_{7-x} Thin Films on Buffered Ni-Based Alloy Substrates, Mat. Res. Soc. Symp. Proc. Vol. 659, High-Temperature Superconductors -- Crystal Chemistry, Processing and Properties, pp. II10.2.1-2.6 (2001), eds. U. Balachandran, H. C. Freyhardt, T. Izumi, and D. C. Larbalestier.

Y. A. Jee, B. Ma, M. Li, B. L. Fisher, and U. Balachandran, Texture Formation and Superconducting Properties of YBa₂Cu₃O_x Thin Films Prepared by Solution Process on LaAlO₃ Single Crystals, Mat. Res. Soc. Symp. Proc. Vol. 659, High-Temperature Superconductors -- Crystal Chemistry, Processing and Properties, pp. II9.17.1-17.6 (2001), eds. U. Balachandran, H. C. Freyhardt, T. Izumi, and D. C. Larbalestier.

J.-H. Park, L. Chen, K. C. Goretta, R. E. Koritala, and U. Balachandran, Oxidation of Hastelloy C276, Paper presented at Cryogenic Engineering Conf. & Intl. Cryogenic Matls. Conf., Madison, WI, July 16-20, 2001.

R. E. Koritala, B. C. Prorok, K. C. Goretta, J.-H. Park, U. Balachandran; and M. J. McNallan (U. of IL at Chicago), Microstructure and Mechanical Properties of Internally Oxidized Ag/1.12 at.% Mg, Paper presented at International Cryogenic Materials Conf., ICMC 2001, Madison, WI, July 16-20, 2001.

M. Li, B. Ma, R. E. Koritala, B. L. Fisher, V. A. Maroni, and U. Balachandran, Structural Characterization of YBCO Films Formed on ISD MgO Buffered Metal Substrate by Pulsed Laser Deposition, Paper presented at Cryogenic Engineering Conf. & Intl. Cryogenic Materials Conf., Madison, WI, July 16-20, 2001.

B. Ma, M. Li, B. L. Fisher, R. E. Koritala, and U. Balachandran, Epitaxial Growth of YBCO Films on Metallic Substrates Buffered with Yttria-Stabilized Zirconia, Paper presented at Cryogenic Engineering Conf. & Intl. Cryogenic Materials Conf., Madison, WI, July 16-20, 2001.

U. Balachandran, M. Li, R. E. Koritala, B. L. Fisher, and B. Ma, Development of YBCO-Coated Conductors for Electric Power Applications, Proc. 5th European Conf. on Applied Superconductivity, Copenhagen, Denmark, Aug. 26-30, 2001.

U. Balachandran, B. Ma, M. Li, B. L. Fisher, R. E. Koritala, R. A. Erck, and S. E. Dorris, Inclined-Substrate Deposition of Biaxially Textured Template for Coated Conductors, Proc. 14th Intl. Symp. on Superconductivity (ISS 2001), Kobe, Japan, Sept. 25-27, 2001.

U. Balachandran, An Overview of Argonne's High- T_c Superconductor Program, Oral presentation at DOE Annual Peer Review, Washington, DC, Aug. 1, 2001.

U. Balachandran, V. A. Maroni, and K. E. Gray, Coated Conductors by Inclined Substrate Deposition: Fabrication and Characterization, Oral presentation at DOE Annual Peer Review, Washington, DC, August 1, 2001.

J. R. Hull, T. M. Mulcahy and R. C. Niemann, Magnetically Levitated Space Elevator to Low Earth Orbit, Abstract presented at the Cryogenic Engineering Conf. and Intl. Cryogenic Matls. Conf. (CEC/ICMC), Madison, WI, July 16-20, 2001.

J. R. Hull and M. Komori (Kyushu Institute of Technology), High Levitation Pressures with Cage-Cooled Superconductors, Paper presented at 3rd Intl. Workshop on Processing and Applications of Superconducting (RE)BCO Large Grain Materials, Seattle, July 11-13, 2001.

J. R. Hull, T. M. Mulcahy and R. C. Niemann (IPNS), Magnetically Levitated Space Elevator to Low Earth Orbit, Paper presented at Cryogenic Engr. Conf., Madison, WI, July 16-20, 2001.

1998-2001 Patents

Thermomechanical means to improve the critical current density of BSCCO tapes
Uthamalingam Balachandran, Roger B. Poeppel, Pradeep Haldar (IGC), and Lesnek Motowidlo (IGC)
U.S. Patent 6,240,619 (June 5, 2001).

Method of manufacturing a high-temperature superconductor with improved transport properties
Uthamalingam Balachandran, Richard Siegel, and Thomas Askew
U.S. Patent No. 6,191,075 (February 20, 2001).

Method and apparatus for measuring gravitational acceleration utilizing a high temperature superconducting bearing
John R. Hull
U.S. Patent 6,079,267 (June 27, 2000).

Engineered flux pinning centers in BSCCO, TBCCO and Y-123 superconductors
Kenneth C. Goretta, Michael T. Lanagan, Jieguang Hu, Dean J. Miller, Suvankar Sengupta, John C. Parker, U. Balachandran, Donglu Shi, and Richard W. Siegel
U.S. Patent 5,929,001 (July 27, 1999).

Passive fault current limiting device
Daniel J. Evans and Yung S. Cha
U.S. Patent 5,892,644 (April 6, 1999).

Automatic HTS force measurement instrument
Scott T. Sanders and Ralph. C. Niemann
U.S. Patent 5,889,397 (March 30, 1999).

Method and etchant to join Ag-clad BSCCO superconducting tape
Uthamalingam Balachandran, A. N. Iyer, and J. Y. Huang
U.S. Patent 5,882,536 (March 16, 1999).

Elongated Bi-based superconductors made by freeze dried conducting powders
Uthamalingam Balachandran, Milan Lelovic, and Nicholas G. Eror
U.S. Patent 5,874,384 (Feb. 23, 1999).

Thin-film seeds for melt processing textured superconductors for practical applications
Boyd W. Veal, Arvydas Paulikas, Uthamalingam Balachandran, and Wei Zhong
U.S. Patent 5,869,431 (Feb. 9, 1999).

Superconductor composite
Stephen E. Dorris, Dominick A. Burlone, and Carol W. Morgan
U.S. Patent 5,866,515 (Feb. 2, 1999).

Surface texturing of superconductors by controlled oxygen pressure
Nan Chen, Kenneth C. Goretta, and Stephen E. Dorris
U.S. Patent 5,856,277 (Jan. 5, 1999).

Method for synthesizing and sinter-forging Bi-Sr-Ca-Cu-O superconducting bars
Nan Chen, Kenneth C. Goretta, and Michael T. Lanagan
U.S. Patent 5,821,201 (Oct. 13, 1998).

Mixed- μ superconducting bearings
John R. Hull and Thomas M. Mulcahy
U.S. Patent 5,722,303 (March 3, 1998).